This paper appears in IEEE Transactions on Medical Robotics and Bionics, 2021.
DOI: 10.1109/TMRB.2021.3050512

Robotic rehabilitation and assistance for individuals with movement disorders based on a kinematic model of the upper limb

Carlos Rossa, Mohammad Najafi, Mahdi Tavakoli, and Kim Adams

***Abstract*—Design and development of robotic-assistance must consider the abilities of individuals with disabilities. In this paper, a 8-DOF kinematic model of the upper limb complex is derived to evaluate the reachable workspace of the arm during interaction with a planar robot and to serve as the basis for rehabilitation strategies and assistive robotics. Through inverse differential kinematics and by taking account the physical limits of each arm joint, the model determines workspaces where the individual is able to perform tasks and those regions where robotic assistance is required. Next, a learning-from-demonstration strategy via a nonparametric potential field function is derived to teach the robot the required assistance based on demonstrations of functional tasks. The paper investigates two applications. First, in the context of rehabilitation, robotic assistance is only provided if the individual is required to move her arm in regions that are not reachable via voluntary motion. Second, in the context of assistive robotics, the demonstrated trajectory is scaled down to match the individual's voluntary range of motion through a nonlinear workspace mapping. Assistance is provided within that workspace only. Experimental results in 5 different experimental scenarios with a person with cerebral palsy confirm the suitability of the proposed framework.**

I. Introduction

SPASTIC movement disorders are prominent features of impaired function of the motor system frequently associated with stroke and cerebral palsy [1]. They are best characterised by changes in reflex excitability, muscle tone, and restricted range of motion, all leading to difficulties in performing voluntary movements [2], [3]. About 460,000 people are living with the effects of stroke in Canada and 770,000 people have one or more symptoms of cerebral palsy in the United States [4], [5]. The limitations in performing voluntary movements restricts people in their daily living activities, but robotics can be used to help build skills (rehabilitation) or to be a tool for people with disabilities to do daily activities (assistive).

Rehabilitation robots help therapists facilitate functional motor recovery of individuals with physical disability [6], [7]. Rehabilitation robots are typically designed for therapeutic exercise, relearning, and reactivating residual motor function while preventing secondary complications such as muscle atrophy [8]. Progressive resistance exercise is a method of increasing the ability of muscles to generate force [9]. Although some symptoms of spasticity are permanent, studies have documented positive effects of robotic-assisted training in improving motor function of individuals living with cerebral palsy [10], and post-stroke movement impairments [11]. For post-stroke therapy, robot-assisted therapy appears to cause more short-term reduction in motor impairment, e.g., muscle activation and speed of movement, than conventional rehabilitation therapy [12]. Different planar robots have been used in recent studies for human upper-limb rehabilitation. The Quanser rehabilitation robot was employed in [13] to evaluate intelligent haptic effectiveness for post-stroke rehabilitation. Using the 2-DOF CASIA-ARM robot, a subject's functional capability was learnt using a Gaussian RBF network and the robot provided assistance according to the subject's performance and condition [14]. The InMotion Arm robot has also been used, and the reliability of measured kinematic variables used in patients' neurorehabilitation after stroke was evaluated [15]. A 2-DOF planar robot detected the correct movements in order to increase the effectiveness of the rehabilitation process [16].

Assistive robots compensate for disability due to a given pathological condition [17]. These technologies are intended to allow individuals to accomplish daily life activities that would otherwise be difficult or impossible to perform, using for example a manipulator arm to interact with a variety of environments and objects [18], [19], [20]. Typically individuals control the manipulator arm using a joystick, but other control interfaces have been tried for individuals with complex physical impairments, including those with stroke and cerebral palsy [21], [22].

Since the symptoms associated with these disorders can vary widely, appropriate interventions must focus on the specific disorders and conditions of each individual [23]. This is particularly relevant for robots used in rehabilitation where quantitative assessment of spasticity is important for evaluating potential effects of treatment [24], guiding the design of a robotic system that complies with the individual's needs and motion tolerances [25], and ensuring individual's safety and comfort during robotic intervention [26]. In particular, it is crucial that the robot be adaptable to the human limb segment lengths, range of motion, forces, and velocity. Furthermore,

This research was supported by the Canada Foundation for Innovation (CFI) under grant LOF 28241, the Alberta Innovation and Advanced Education Ministry under Small Equipment Grant RCP-12-021, the Natural Sciences and Engineering Research Council (NSERC) of Canada, the Canadian Institutes of Health Research (CIHR), and Quanser, Inc.

C. Rossa, M. Najafi, and M. Tavakoli are with the Department of Electrical and Computer Engineering, University of Alberta, Edmonton, Canada. E-mail: rossa@ualberta.ca; najafi@ualberta.ca; mahdi.tavakoli@ualberta.ca.

K. Adams is with the Faculty of Rehabilitation Medicine at the University of Alberta, and with the Glenrose Rehabilitation Hospital, Edmonton, Canada. E-mail: kdadams@ualberta.ca.

when designing robotic rehabilitation strategies, clinical standards must be considered in order to retain compatibility with traditional therapies while involving a minimum amount of robot programming and adjustments.

From the above discussion one can infer that in implementing assistive and rehabilitation robotics, assessing the individual's pathological conditions is the very first step. A variety of assessments exist to quantify spasticity [27]. The most common techniques quantify the velocity-dependent response of muscle to passive stretching. One method that has been extensively used clinically involves manually moving a limb through its range of motion and grading the resistance encountered on a five-point ordinal scale [28]. In more sophisticated methods, servo-controlled motors apply controlled displacement or torque to joints while limb angle, torque, and electromyographic response are recorded [24]. Other measures such as range of motion of each joint achieved with assistance and without assistance according to the individual's tolerances may be included in these metrics.

Based on the identified range of each joint, a kinematic model of the upper limb can be used to identify workspaces where the individual with disability is able to perform tasks, and those regions where assistance is required. Robotic intervention strategies can then be established based on an individual's specific capabilities. Upper limb models in biomechanics typically use 7 degrees of freedom (DoF), 3 DoF for the shoulder, 2 DOF in the elbow joint and 2 DoF in the wrist joint [27]. To extend the model to fit our purpose we propose a kinematic structure exhibiting 8 DoF.

Knowing an individual's workspaces opens up two possibilities. The first possibility relates to rehabilitation. It is assumed that an individual is able to move her arm in a given workspace that can be determined through the kinematic model. Robotic assistance is only provided when she is required to move her arm in a region she is not able to reach without assistance. Rather than pre-programming robot movements for therapy, a therapist can demonstrate a desired trajectory to the individual while using a robot, and the robot can calculate the required assistance. Then, in the therapist's absence, the robot provides the same assistance the individual received during the task demonstration. It should be noted that the robotic rehabilitation approaches above [13], [14], [15], [16] do not take into consideration the kinematics of the user's arm, i.e., range of motion etc. In our proposed approach a kinematic model of the upper limb informs the controller about the capabilities and range of motion of the user and motion planning or assistance are then designed based on the information acquired from the model

The second possibility concerns assistive robotics. To engage individuals with disabilities, they should do as much of an activity as they can. However, they may need assistance to be accurate with some tasks. One way to provide assistance is for a helper to demonstrate the desired robot movements, the robot learns the necessary assistance, and then the individual with the disability does the task independently in cooperation with the robot. This scheme can either involve a single robot or a telerobotic system (with positions and interaction forces of the two robots correlated to one another through control). In both cases, the individual with the disability holds the robot to receive assistance for tasks through haptic guidance. Since the workspace of the individual with disabilities is likely different from that of the helper, motion scaling may be needed. Thus, tasks being demonstrated in regions that the individual cannot reach can be scaled to match their feasible range of motion, so as not to pose any risk or discomfort to the individual with the disability. Workspace mapping has been used in some robotic studies to facilitate patient/therapist task completion. Scaling has been implemented to help patients span a wider manipulating workspace [29]. Nonlinear mapping strategies have utilized Cartesian to Cartesian [30] and Normal-tangential to Cartesian [31] mapping approaches. A hybrid method that switches between joint space and operating space mapping methods has also been used to address user and environment robot workspace differences [32]. However, they have not been tailored specifically to the workspace of the individual from a kinematic model.

In this paper we develop the strategies described above, organized around three main contributions: 1) A 8 degrees-of-freedom (DOF) kinematic model of the upper limb is derived to evaluate the individual's range of motion. This is achieved through inverse differential kinematics taking into account the physical limits of each joint. 2) A learning-from-demonstration strategy via a nonparametric potential field function that teaches the rehabilitation robot the required assistance based on the demonstration from a therapist and applies assistence where needed, and 3) A method to map different workspaces allowing two individuals to control an assistive robot while limiting the individual's motion to her feasible range. As the reader will notice, these contributions do not depend on each other and may be used independently.

II. Kinematics of the Upper Limb

As a first approximation, a reasonable assumption to model the mechanical structure of the human arm complex is to consider it to be composed of 8 degrees of freedom (DOF). As shown in the left part of Fig. 1, it is appropriate to model the human arm as a triple-pendulum whose segments are the humerus, the forearm, and the hand, connected through the appropriate number of revolute joints [33], [34]. From the kinematic point of view, it is convenient to single out 4 DOF at the shoulder to allow for shoulder retraction/protraction, glenohumeral internal/external rotation, glenohumeral elevation through the adduction and abduction, and humeral retroflexion/flexion, 1 DOF at the elbow allowing for extension and flexion of the forearm, and 3 DOF at the wrist, allowing for wrist supination/pronation, flexion/extension, and radial/ulnar deviation. Depression/elevation of the shoulder is neglected because the proposed tasks are in a horizontal plane with a planar robot. In Fig. 1, ℓ_0 is the acromiohumeral interval, ℓ_1 and ℓ_2 are the length of the humerus and forearm, respectively, and ℓ_3 is the distance from the distal palmar crease to the wrist crease.

The equivalent kinematic model consisting of 8 revolute links is presented in the right part of Fig. 1. A base inertial frame $x_0y_0z_0$ is fixed at the shoulder glenoid cavity. Local body

NOMENCLATURE

Section II

$x,\ y,\ z$	Three-dimensional Cartesian coordinates
ϑ_i	Angle of rotation of joint i about axis z_{i-1}
$q \in \mathbb{R}^{8\times 1}$	Vector of joint space coordinates
$\varphi(q),\ \psi(q)$	Roll and pitch of the hand w.r.t y_0 and x_0
$p \in \mathbb{R}^{5\times 1}$	Vector of task space coordinates
α_i	Twist angle between axes z_{i-1} and z_i about x_i
a_i	Length of link i along axis x_i
d_i	Distance of joints i and $i-1$ about z_{i-1}
A_i^{i-1}	Transformation from frame i to frame $i-1$
$T_i^0 \in \mathbb{R}^{4\times 4}$	Transformation from frame i to base frame
r_{ab}	Element in the a^{th} row and b^{th} column of T_i^0
$\ell_0, \ell_1, \ell_2, \ell_3$	Length of upper limb segments
$\Gamma(q)$	Forward kinematics function
$\dot{q},\ \dot{p}$	Joint space velocities, and Cartesian velocity
$J(q) \in \mathbb{R}^{5\times 8}$	Jacobian matrix $\partial\Gamma(q)/\partial q$
$\vartheta_i^0,\ \vartheta_i^u,\ \vartheta_i^l$	Rest, maximum, and minimum angle of joint i
$\upsilon(\vartheta),\ \zeta(\upsilon)$	Conversion function of angles, and its inverse
$d\zeta \in \mathbb{R}^{8\times 8}$	Weighing matrix of the transformed Jacobian
$J_c^{\dagger}(\upsilon)$	Damped pseudoinverse of transformed Jacobian
$\mu \in \mathbb{R}^{+}$	Damping coefficient of peudoinverse Jacobian
$\hat{p},\ \hat{\upsilon}$	Desired Cartesian trajectory and joint angles
$k_0 \in \mathbb{R}^{+}$	Inverse kinematics control gain constant

Section III

$\xi_t \in \mathbb{R}^{2\times 2}$	Reference attractor points
ξ_ℓ	Distance from target along reference trajectory
$\phi_j(\xi),\ \Phi(\xi)$	Local and total potential energy field
ϕ_{0_j}	Potential field bias
$S \in \mathbb{R}^{2\times 2}$	Diagonal matrix used to scale $\phi(\xi)$
$\omega_j(\xi)$	Weight assigned to attraction point j
$\sigma \in \mathbb{R}^{+}$	Gaussian kernel smoothing parameter
$\lambda,\ \Lambda$	Local and total dissipative fields
$D \in \mathbb{R}^{2\times 2}$	Diagonal matrix of damping coefficients
$k_1 \in \mathbb{R}^{+}$	Scalar constant
$F \in \mathbb{R}^{2\times 1}$	Robot applied force at ξ

Section V

$\xi = [x\ y]^T$	Vector of planar task space coordinates
$g(\xi)$	Two-dimensional interpolation function
$W_r,\ W_c$	Regular and constrained workspaces
$\xi_r,\ \xi_t$	Landmarks in each workspaces
R, Q	Vectors or reference and target landmarks
b_0, b_1, b_2	Uniform transformation coefficient vectors
w_i	n nonuniform transformation weights
v_{ij}	Euclidean distance between two points
$U,\ K$	Radial basis function and its matrix form
O_1, O_2	Matrices of zeros
L	Energy required to displace landmarks

frames $x_iy_iz_i$, $i = 1,2,...8$, are fixed at the origin of link $i+1$. Frame $i = 8$ is at the center of the hand and corresponds to the position of the end-effector. Following the Denavit-Hartenberg convention (DH) [35], axis i denotes the axis of the joint connecting link $i-1$ to link i. The angle of rotation of link i about the axis z_{i-1} is ϑ_i. Let a_i be the length of link i, i.e., the distance between z_{i-1} and z_i axes along x_i, and d_i the joint distance, i.e., the distance between x_{i-1} and x_i about z_{i-1}. Let also α_i be the twist angle between axes z_{i-1} and z_i about x_i.

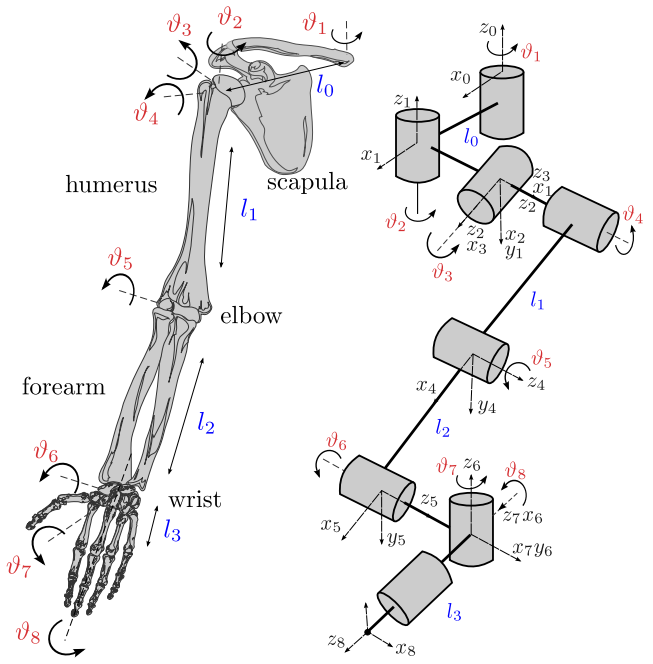

Fig. 1. Overview of the upper limb segments and joints (left), and the equivalent 8-DOF kinematic model (right) (not in scale).

The transformation matrix A_i^{i-1} from frame i to frame $i-1$ is

$$A_i^{i-1}(q) = \begin{bmatrix} \mathbf{C}\vartheta_i & -\mathbf{S}\vartheta_i\,\mathbf{C}\alpha_i & \mathbf{S}\vartheta_i\,\mathbf{S}\alpha_i & a_i\mathbf{C}\vartheta_i \\ \mathbf{S}\vartheta_i & \mathbf{C}\vartheta_i\,\mathbf{C}\alpha_i & -\mathbf{C}\vartheta_i\,\mathbf{S}\alpha_i & a_i\mathbf{S}\vartheta_i \\ 0 & \mathbf{S}\alpha_i & \mathbf{C}\alpha_i & d_i \\ 0 & 0 & 0 & 1 \end{bmatrix}, \quad (1)$$

where $q = [\vartheta_1\ \ \vartheta_2\ \ ...\ \ \vartheta_8]^T \in \mathbb{R}^{8\times 1}$ is the vector of joint variables. Hereafter, shorthand notations $\mathbf{S}$ and $\mathbf{C}$ describe $\sin(\cdot)$ and $\cos(\cdot)$, respectively. In this section, the subscript of a vector or matrix denotes the frame in which its components are expressed.

The DH parameters for the 8-link mechanism to be used in (1) are summarised in Table I (The values are multiples of 10 for simplicity). It is worth noting that the shoulder and the wrist have spherical joints since all of their respective revolute axis intersect at a single point and thus a_2, a_3, a_4, and a_6, a_7, a_8 equal zero. The center of rotation of the humerus is shifted from the rotation axis of the scapula joint by ℓ_0 and thus $d_1 = \ell_0$. Likewise, the end-effector is shifted from the center of rotation of the wrist by ℓ_3 and hence $d_8 = \ell_3$. For the 8-link mechanism, it follows that the coordinate of a point $p^j = [x_j\ y_j\ z_j\ 1]^T$, expressed in frame j with respect to the base frame can be calculated as

$$p^0 = \prod_{i=1}^{j} \left[A_i^{i-1}(q_i)\right] p^j = T_j^0(q) p^j. \quad (2)$$

The x,y,z position of the end-effector in the inertial frame is

$$[x\ y\ z\ 1]^T = T_8^0(q)[0\ 0\ 0\ 1]^T, \quad (3)$$

with $T_8^0 \in \mathbb{R}^{4\times 4}$ being defined in (2). The 3D position of the hand as a function of the joint angles is now known. In order to fully specify the pose of the hand, one must also determine its orientation in the base frame. To this end, consider that the

TABLE I
DH PARAMETERS FOR THE 8-LINK HUMAN ARM MODEL(PERSON WITH CEREBRAL PALSY IN EXPERIMENTS) IN REGULAR AND RESTRICTED RANGE OF MOTION W.R.T THE REST ANGLE ϑ_i^0. ANGLES ARE IN DEGREES.

Joint	Motion	ϑ_i	a_i	α_i	d_i
1	Scapular retraction	ϑ_1	ℓ_0	0	0
2	Glenohumeral rotation	ϑ_2	0	-90	0
3	Shoulder adduction	ϑ_3	0	-90	0
4	Humeral flexion	ϑ_4	ℓ_1	0	0
5	Forearm extension	ϑ_5	ℓ_2	0	0
6	Wrist flexion	ϑ_6	0	90	0
7	Wrist deviation	ϑ_7	0	-90	0
8	Wrist supination	ϑ_8	0	0	ℓ_3

	ϑ_1	ϑ_2	ϑ_3	ϑ_4	ϑ_5	ϑ_6	ϑ_7	ϑ_8
ϑ_i^0	180	0	90	0	0	0	-90	0
ϑ_i^l	-10	-20	50	20	0	-50	-30	10
ϑ_i^u	15	10	90	80	70	60	-45	50
ϑ_i^0	180	0	90	0	0	0	-90	0
ϑ_i^l	0	0	70	30	30	30	-30	40
ϑ_i^u	0	5	90	70	60	60	-30	45

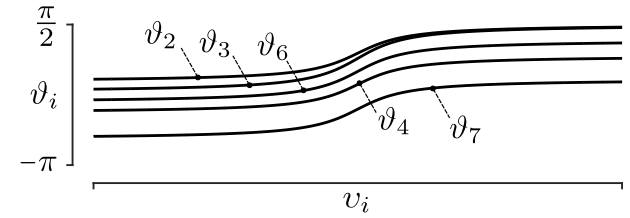

(a) Saturation function of joint angles

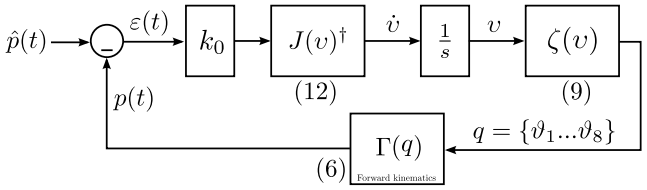

(b) Overview of the constrained differential inverse kinematics

Fig. 2. Overview of the inverse kinematics formulation with joint limits. In (a) the each curve shows the transformed joint angle ϑ_i as a function of the new variable ϑ_i for the joint limits given in Table I. In (b), the differential kinematics workflow is shown.

user interacts with a planar robotic manipulator.

A. Scleronomic Constraints

Without loss of generality, suppose that an individual interacts with a planar robot whose end-effector translates on the (x_0, y_0) plane and is placed at a fixed distance along z_0. Also, assume that the end-effector has a handle that is normal to that plane (parallel to z_0). Let $r_{a,b}$ denote the element in the a^{th} row and b^{th} column of the transformation matrix T_0^8 defined in (2). When the individual holds the robot's handle, the roll $\varphi(q)$ of his hand (angle with respect to x_0) and its pitch $\psi(q)$ (angle with respect to y_0) are invariant in time and given as

$$\varphi(q) = \tan^{-1}\left(\frac{r_{3,2}}{r_{3,3}}\right) = 0, \tag{4}$$

$$\psi(q) = \tan^{-1}\left(-\frac{r_{3,1}}{\sqrt{(r_{3,2})^2 + (r_{3,3})^2}}\right) = -\frac{\pi}{2}, \tag{5}$$

Note that no constraint is imposed on the hand's yaw. This allows introducing the task space vector that specifies the hand's position (x, y, z) and orientation (φ, ψ) denoted $p \in \mathbb{R}^{5\times 1}$ and defined as $p = [x\ y\ z\ \varphi\ \psi]^T$.

B. Forward Kinematics

The direct kinematics equation specifies the relationship between the joint vector q and the Cartesian vector p as

$$p = \Gamma(q). \tag{6}$$

Analogously, the relationship between the joint velocities $\dot{q}$ and Cartesian velocities $\dot{p}$ is obtained as

$$\dot{p} = J(q)\dot{q}, \tag{7}$$

where the dot operator $\dot{(\,)}$ denotes the derivative with respect to time t, and $J(q) \in \mathbb{R}^{5\times 8}$ is the Jacobian matrix $\partial\Gamma(q)/\partial q$.

It is now clear that the 8-DOF arm is kinematically redundant since the 5 variables specified in Cartesian space depend each on 8 independent joint space variables [36].

C. Differential Inverse Kinematics

To compute the posture of the upper limb when the hand follows a specific trajectory, the inverse kinematics must guarantee that each joint stays within its physical limits. This can be achieved through a transformation of variables that will bring the joint angles into a new variable, using a function that saturates a joint angle when it approaches a given limit.

Let ϑ_i^u and ϑ_i^l be the upper and lower limits of joint i (see Table I for numerical values of an adult individual with cerebral palsy). The function that transforms the joint variables to a new variable $\upsilon_i = f(q)$ must be continuously increasing in the open interval $(\vartheta_i^l, \vartheta_i^u)$. A suitable candidate for this function is the tangent function $\tan(\theta_i)$, where θ_i is linearly mapped from $(\vartheta_i^l, \vartheta_i^u)$ to $(-\pi/2, \pi/2)$, that is:

$$\upsilon_i(\vartheta_i) = \tan\left(\frac{\pi}{2}\frac{2\vartheta_i - \vartheta_i^u - \vartheta_i^l}{\vartheta_i^u - \vartheta_i^l}\right), \tag{8}$$

and whose inverse

$$\zeta(\upsilon_i) = \theta_i(\upsilon_i) = \frac{\vartheta_i^u - \vartheta_i^l}{\pi}\tan^{-1}(\upsilon_i) + \frac{\vartheta_i^u + \vartheta_i^l}{2} \tag{9}$$

is bounded to $(\vartheta_i^l, \vartheta_i^u)$ as shown in Fig. 2(a) for the joint limits given in Table I. This will ensure that the joint limits will not exceed their specified limits in the formulation of the inverse kinematics.

Now, one can substitute (9) into the forward kinematics given in (7) and recompute the Jacobian with respect to the new variable $\upsilon = [\upsilon_1\ \upsilon_2\ \cdots\ \upsilon_8]^T$. The new Jacobian $J_c(\upsilon)$ is

calculated as $\partial\Gamma(\upsilon)/\partial\upsilon$, which is equivalent to setting

$$J_c(\upsilon) = \begin{bmatrix} \frac{\partial x(\upsilon)}{\partial \upsilon_1} & \frac{\partial x(\upsilon)}{\partial \upsilon_2} & \cdots & \frac{\partial x(\upsilon)}{\partial \upsilon_8} \\ \frac{\partial y(\upsilon)}{\partial \upsilon_1} & \frac{\partial y(\upsilon)}{\partial \upsilon_2} & \cdots & \frac{\partial y(\upsilon)}{\partial \upsilon_8} \\ \frac{\partial z(\upsilon)}{\partial \upsilon_1} & \frac{\partial y(\upsilon)}{\partial \upsilon_2} & \cdots & \frac{\partial y(\upsilon)}{\partial \upsilon_8} \\ \frac{\partial \varphi(\upsilon)}{\partial \upsilon_1} & \frac{\partial \varphi(\upsilon)}{\partial \upsilon_2} & \cdots & \frac{\partial \varphi(\upsilon)}{\partial \upsilon_8} \\ \frac{\partial \psi(\upsilon)}{\partial \upsilon_1} & \frac{\partial \psi(\upsilon)}{\partial \upsilon_2} & \cdots & \frac{\partial \psi(\upsilon)}{\partial \upsilon_8} \end{bmatrix} = J(q)d\zeta, \quad (10)$$

where the term $d\zeta \in \mathbb{R}^{8\times 8}$ is

$$d\zeta = \begin{bmatrix} \frac{\partial \zeta(\upsilon)}{\partial \upsilon_1} & 0 & \cdots & 0 \\ 0 & \frac{\partial \zeta(\upsilon)}{\partial \upsilon_2} & \cdots & \vdots \\ \vdots & 0 & \ddots & 0 \\ 0 & \cdots & 0 & \frac{\partial \zeta(\upsilon)}{\partial \upsilon_8} \end{bmatrix}. \quad (11)$$

The inverse solution of (7) can now be written considering the change of variables and the saturation of the joint angles as

$$\dot{\upsilon} = J_c^{\dagger}(\upsilon)\dot{p}, \quad (12)$$

where $J_c^{\dagger}(\upsilon)$ is the damped pseudoinverse of the transformed Jacobian matrix given by

$$J_c^{\dagger}(\upsilon) = J_c(\upsilon)^T[J_c(\upsilon)J_c(\upsilon)^T + \mu I]^{-1} \quad (13)$$

if the Jacobian is full rank, providing a least-squares solution with minimum norm to (7). In (13), $I \in \mathbb{R}^{5\times 5}$ is an identity matrix and $\mu \in \mathbb{R}^+ << 1$ is the damping constant scalar used to avoid possible discontinuity of the pseudoinverse at a singular configuration. In detail, this solution satisfies the condition $\min\|\dot{\upsilon}\|$. Furthermore, provided that $\zeta(\upsilon)$ is monotonically increasing in the open interval $(\vartheta_i^l \;\; \vartheta_i^{\mu})$, and given that $\dot{\upsilon} = \dot{f}(q)\dot{q}$, the pseudoinverse Jacobian also satisfies $\min\|\dot{q}\|$.

Let $\hat{\upsilon}(t)$ be a solution to $\hat{p}(t) = \Gamma(\upsilon)$ relative to a desired Cartesian trajectory $\hat{p}(t) \in \mathbb{R}^{5\times 1}$. A purely proportional control law in the form of

$$\dot{\upsilon} = k_0 J_c^{\dagger}(\upsilon)[\hat{p}(t) - \Gamma(q)], \quad (14)$$

can be shown to ensure that $\varepsilon = \hat{p}(t) - \Gamma(q) \to 0$, and then $\upsilon \to \hat{\upsilon}$, provided that $k_0 > 0$. It is important to underscore that $\Gamma(q)$ is the forward kinematics computed with the physical joint angles ϑ_i calculated through the inverse transformation $q = \zeta(\upsilon)$ using (9). Obviously, the maximum tracking error ε depends on $\dot{\hat{p}}$, and inversely on $k_0 \in \mathbb{R}^+$, however the steady-state error (ε when $\dot{\hat{p}} = 0$) is zero [37]. Fig. 2(b) summarizes the closed-loop differential kinematics workflow incorporating the joint limits.

Here we shall make four remarks before moving forward:

1) Close scrutiny of (13) reveals that $J_c(\upsilon)^{\dagger} = J(q)^{\dagger}d\zeta^{-1}$ (for $\mu = 0$), meaning that the transformation of variable acts as a gain in the velocity of joints and stiffens those that are close to their limits.
2) The formulation in (14) implies that the arm tends to move from an initial point $\hat{p}(t = t_0)$ to a new point $\hat{p}(t = t_1)$ following a trajectory that minimizes the joint velocities. In other words, the hypothesis is that trajectories are chosen to minimize metabolic energy costs, as supported by [38], [39].
3) Because of 2), a trajectory between two points is likely to be a straight line. To accurately represent the human behaviour, point-to-point motion was approximately considered a collection of straight segments.
4) The boundaries of the workspace calculated through the model do not depend on 2) nor 3).

D. Regular and Constrained Workspaces

Given the joint limits and the inverse kinematic model, one can determine the reachable workspace of the arm when interacting with a planar robot (with scleronomic constraints defined in Section II-A).

A 50 year old adult who has quadreplegic cerebral palsy with mixed high and low muscle tone and involuntary movements was recruited as a participant for this study. She has been classified as Level IV in the Gross Motor Function Classification System Expanded and Revised (GMFCS-ER) [40], meaning that she performs self-mobility by using a powered wheelchair, and Level III according to the Manual Ability Classification System (MACS) [41], meaning she has difficulty handling objects.

The participant moved a 2D planar robot as much as she could in each direction. Due to spasticity and hypertonia she was uncomfortable and uncoordinated when rotating the joints more than a certain angle while performing a task. The grey volume shown in Fig. 3(a) is the reachable space for the individual based on the observed limits given in Table I, and her arm segments length of $l_0 = 130$, $l_1 = 290$, $l_2 = 300$, and $l_3 = 70$ mm. And, the red volume in Fig. 3(a) based on the observed limits given in Table I, demonstrates the range where the adult with cerebral palsy felt comfortable and coordinated to perform the task.

We are now in a position to reinforce the concepts of *constrained* and *regular* ranges of motion. The former refers to the workspace when one or more joints have limited range of motion but the user feels comfortable and coordinated moving the limb. The later is the range that the individual may feel uncomfortable or uncoordinated reaching, but the points may be attained by means of robotic assistance if the arm is stretched without causing pain or discomfort. A horizontal cross section of these ranges when the robot was placed at $z = -240$ mm below the shoulder is shown in Fig. 3(b). The respective surfaces will be denoted W_c (constrained) and W_r (regular).

III. Robot Control and Potential Fields

The next subsystem of the proposed framework for assistive and rehabilitation robotics is the algorithm that calculates the required robotic assistance. Typically, variable impedance controllers have been used to regulate interaction between the human and a robotic manipulator [42], [43]. The term interaction impedance defines the ratio of applied force to the magnitude of deviation from the reference trajectory. It allows adapting the robot properties by making it more or less compliant in certain regions, while cooperatively accomplishing a task such as following a given path [44], [45]. Variable

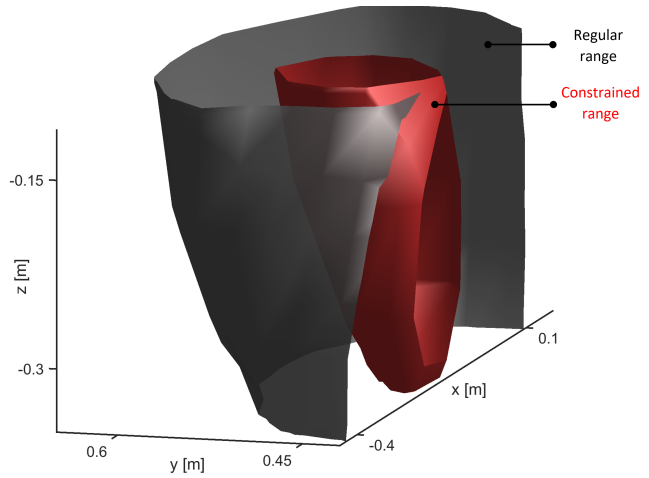

(a) Regular workspace (grey) and constrained workspace (red)

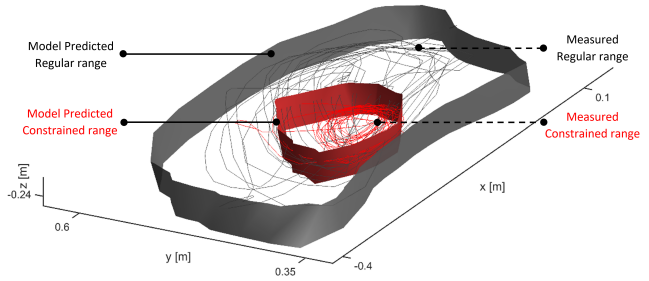

(b) Hozirontal cross section of the workspace in (a) at $z = -250$ mm.

Fig. 3. Reachable workspaces during interaction with a planar robot. The grey volume in (a) represents the workspace an individual without disability can reach. The red volume is the reachable workspace when the elbow is flexed at $110^\circ \pm 2^\circ$. A vertical cross section of (a) is shown in (b) for $z = -250$ mm. The model predicted ranges match with the measured ranges by the participant with cerebral palsy

impedance control relies on position control and hence, real-time motion generation that operates jointly with the controller is needed. Rather than a position controller, we intend to calculate the required assistance (e.g., the required force to keep the robot end-effector within the desired trajectory and/or moving toward the desired endpoint) based on trajectories that a therapist demonstrates to the robot. To this end, we will adapt the nonparametric potential field function first introduced in [46]. The robot position and impedance are captured by the potential function's gradient and curvature. Then, in the therapist's absence, the robot provides the individual with the same assistance received during the task demonstration. This time-invariant controller with bounded force range guarantees that the robot is stable when in contact with passive environments.

Any functional task can be decomposed into a set of motion primitives. Thus, a task is assumed to consist in following a reference trajectory given by a combination of m discrete points in the 2D space denoted by $\xi_{t_j} = [x_t \; y_t]^T$ with $1 \leq j \leq m$. This trajectory ends at the location of a target point ξ_{t_m}. The objective of the algorithm is to calculate the necessary forces to be applied by the robot such that ξ_e is attracted toward ξ_t.

A point ξ is associated to an energy element $\phi_j(\xi)$ that

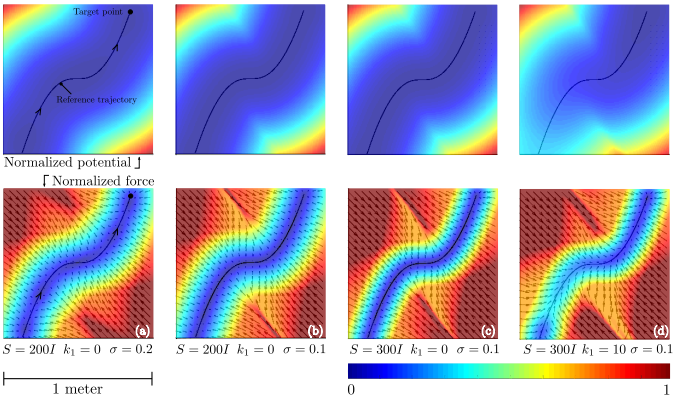

Fig. 4. Normalized potential field (first row) and resulting force (second row) for a hypothetical trajectory. Colours give magnitude and arrows indicate force direction. From (a) to (b) only σ changes and reduces the smoothness of the force. From (b) to (c), S increases and so does the force magnitude. From (c) to (d) only k_1 changes to orient the force toward the target point.

quantifies its attraction to the j^{th} reference point ξ_{t_j}, that is

$$\phi_j(\xi) = \phi_{0_j} + \frac{1}{2}(\xi - \xi_{t_j})^T S(\xi - \xi_{t_j}), \tag{15}$$

where $\phi_0 \in \mathbb{R}$ is a constant scalar, and $S \in \mathbb{R}^{2\times 2}$ is a positive definite diagonal matrix. The force attracting the point ξ to each of the reference points ξ_{t_j} is $S(\xi - \xi_{t_j})$. Thus, the higher S, the higher the attraction force applied *normal* to the reference trajectory. Similarly, ϕ_{0_j} adjusts the magnitude of the force applied *tangentially* to the reference trajectory at ξ_{t_j}. Since the resultant attraction force depends on m reference points, the contribution of each reference point in the force magnitude and direction is calculated using the Gaussian kernel

$$\omega_j(\xi) = e^{-\frac{1}{2\sigma^2}(\xi - \xi_{t_j})^T(\xi - \xi_{t_j})}. \tag{16}$$

Here, $\sigma \in \mathbb{R}^+$ is a smoothing parameter that gives the region of influence of each reference point ξ_{t_j}. The total potential energy at ξ is the weighted average

$$\Phi(\xi) = \frac{\sum_{j=1}^m \omega_j(\xi)\phi_j(\xi)}{\sum \omega_j(\xi)}. \tag{17}$$

Similarly, we can associate a dissipative field $\lambda(\dot{\xi})$ to a point ξ that depends on the end-effector velocity $\dot{\xi}$ as

$$\lambda(\dot{\xi}) = D\dot{\xi} \tag{18}$$

with $D \in \mathbb{R}^{2\times 1}$ being a positive definite damping matrix. Analogously to the average potential energy, the total dissipative energy is computed through the weighted sum of dissipative elements for each attractor point ξ_t as

$$\Lambda(\xi, \dot{\xi}) = \frac{\sum_{j=1}^m \omega_j(\xi)\lambda(\dot{\xi})}{\sum_{j=1}^m \omega_j(\xi)}. \tag{19}$$

Alternatively, for simplicity, a constant damping may be applied through the robot impedance controller.

The force $F \in \mathbb{R}^{2\times 1}$ applied at ξ that attracts the end-effector to the reference trajectory is given as the negative

(a) Experimental setup

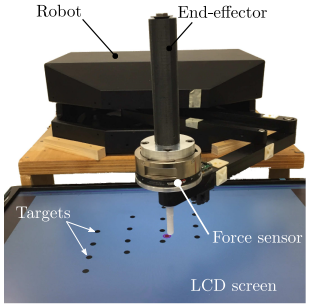

(b) Planar rehabilitation robot with LCD screen

Fig. 5. Experimental setup. Fig. (a) shows our participant with cerebral palsy holding the planar rehabilitation robot. Fig. (b), shows the planar rehabilitation robot with a LCD mounted screen used in the experiments.

gradient of $\Phi(\xi)$ minus the dissipative field $\Lambda(\xi,\dot{\xi})$, i.e.,

$$F(\xi,\dot{\xi}) = -\nabla\Phi(\xi) - \Lambda(\xi,\dot{\xi}). \tag{20}$$

Note that F is a two dimensional vector whose magnitude at ξ is $\|F(\xi,\dot{\xi})\|$.

Back to Equation (15), we still have to define the constants ϕ_0 in order to adjust the magnitude of the force the robot applies tangentially to the reference trajectory, i.e., the force that pulls the user's hand toward the target point. By postulating that this force should increase with the distance from the target, we set

$$\phi_{0_j} = k_1 \xi_{\ell_j}^2. \tag{21}$$

Here, $k_1 \in \mathbb{R}$ is a scalar constant and ξ_{ℓ_j} is the distance of the reference point ξ_r from the target point computed along the reference trajectory, i.e.,

$$\xi_{\ell_j} = \|\xi_{t_j} - \xi_{t_{j+1}}\| + \xi_{\ell_{j+1}} \tag{22}$$

with $\xi_{\ell_{j=m}} = 0$. The constant k_1 shall not be confused with S in (15), which rather defines the magnitude of the force that pulls the end-effector position toward the reference trajectory. For $k_1 = 0$, as long as the robot's end-effector lays anywhere on the reference trajectory, the force $F(\xi,\dot{\xi}=0)$ is zero.

Fig. 4 shows an example of the potential field and the resulting force for a hypothetical reference trajectory for different parameters S (in (15), it controls potential field intensity), σ (in (16), it defines field smoothness), and k_1 (in (21), it controls dragging force).

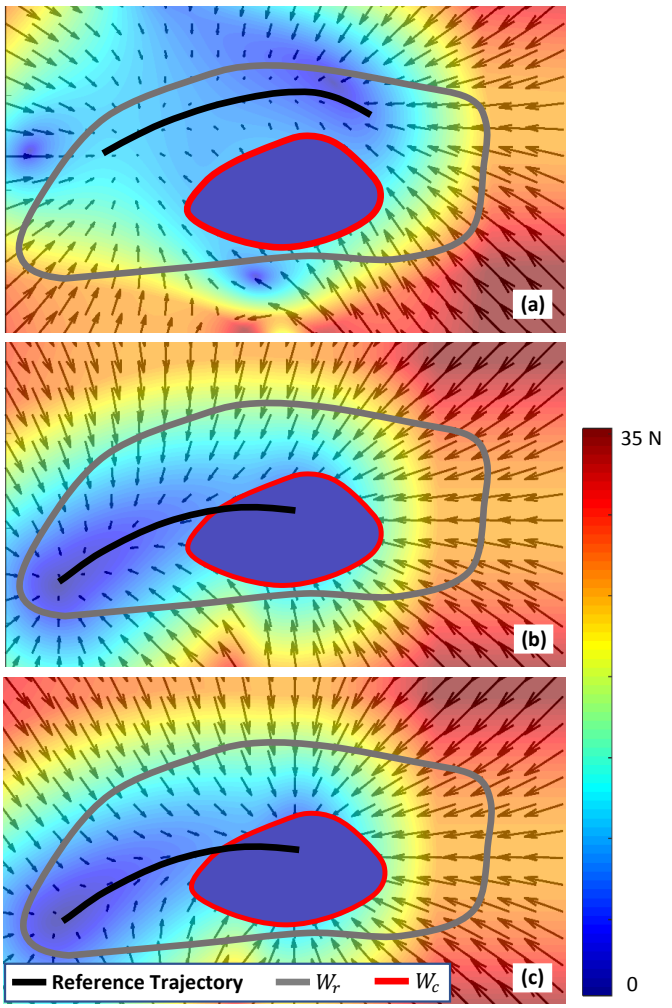

Fig. 6. Force field for Scenarios 1 (stretching the arm, Fig. (a)), 2 (providing assistance, Fig. (b)) and 3 (resisting against the motion, Fig. (c)). The force is zero within the constrained workspace. In (a), if the individual approaches the limit of the constrained workspace, the end-effector is attracted to the closest point on the reference trajectory. In (b), the force field converges to the trajectory end-point. In (c), the field acts against the individual's motion towards the end-point. See Table II for potential field parameters.

IV. Application to Robotic Rehabilitation

The objective now is to combine the workspaces computed through the kinematic model with the robot force controller to create an algorithm that provides robotic assistance as the individual performs a task. In what follows, consider the experimental setup shown in Fig. 5. The individual with cerebral palsy interacts with a planar rehabilitation robot (Stroke rehab robot from Quanser Inc, Markham, ON, CA). The individual positioned her wheelchair in front of the planar robot, and grasped the end-effector with her dominant hand (i.e., left hand). A force sensor (Gamma SI-32-2.5, from ATI Inc, Goodworth, NC, USA) is connected to the end-effector in order to measure the force applied between the individual and the robot. The 2D position of the end-effector is the input to the potential field function, which outputs the desired force to be applied at that location. Force is then controlled using a closed-loop proportional-integral controller. To avoid excessive forces the potential field can be adjusted

in two ways. First an upper bound can be defined so that the force anywhere on the workspace does not exceed that maximum value. Second, the smoothness of the force field can be adjusted to avoid sudden changes in force magnitude throughout the workspace.

A LCD screen was placed below the planar robot end-effector to display in real-time the position of the robot's end-effector and target points and/or trajectories with proper scaling and orientation. In a rehabilitation paradigm, it is considered that the individual is able to perform tasks in the constrained workspace (W_c) and assistance must be provided only when the individual is required to reach points in the regular workspace. This means:

$$\begin{cases} S=0,\ k_1=0 & if \quad \xi \in W_c \\ S>0,\ k_1\neq 0 & \text{otherwise} \end{cases} \tag{23}$$

Three experimental scenarios are designed:

1) **Scenario 1 - Stretching the arm**: Start and end points are displayed on the monitor, and the individual moves towards them at her own pace. No assistance is provided as the user moves her arm within the constrained workspace. When the individual approaches the boundaries of that workspace, the arm is pulled and stretched toward the nearest point on a target trajectory (see Fig. 6(a)).
2) **Scenario 2 - Assistive therapy**: A therapist defines a trajectory that the individual is required to follow and reach its end point located outside her constrained range of motion. The trajectory is displayed on the monitor, and the individual follows it from right to left at her own pace. Assistance is provided as the individual approaches the limit of the constrained workspace (see Fig. 6(b)).
3) **Scenario 3 - Resistive therapy**: The therapist defines a trajectory, which is displayed on the monitor, and the individual follows it from right to left at her own pace. As opposed to Scenario 2, the robot applies forces against the individual's motion in a rate that *increases* as she approaches the target point. This is achieved by setting $k_1 < 0$ and $S > 0$ with $-k_1 < S$. In Fig. 6(c) observe how the potential field prevents the user from deviating from the trajectory while opposing the motion toward the target point.

Fig. 7 summarizes the experimental results. The results for Scenario 1 are shown in the first column of Fig. 7. The first row shows the trajectory followed by the individual toward the reference dashed line located outside the constrained rage of motion. As can be noted in the middle row, the magnitude of the force applied by the robot ($\|F(\xi,\dot{\xi})\|$) is zero when the end-effector is within the constrained range of motion. It increases when the individual reaches the limit of her feasible range bringing the end-effector towards the nearest point on the target line. The third row shows the magnitude of the measured velocity. Similarly, the results for Scenario 2 can be seen in the second column of Fig. 7. Notice how each of the 4 trials converges at the same endpoint of reference trajectory since $k_1 > 0$. See Table II for details of the force field parameters. As opposed to Scenarios 1 and 2, in Scenario 3 the robot is making the task harder for the individual in Fig. 7(c). It is worth noticing that the highest force is applied near the target point.

All the scenarios considered here are in the context of rehabilitation, where the individual is solicited to perform a task outside of her voluntary range of motion. In other instances such as in assistive robotics for common daily tasks, it is preferable to limit the individual's motion to his voluntary range. This will be addressed in the next section.

V. Workspace Mapping

Consider now that the individual interacts with another individual through a teleoperated robotic scheme. Since the individual's workspace may be different from the workspace of the required task, motion may be scaled according to a mapping from the device position. The idea is that motion executed in one workspace using one of the manipulators is scaled up or down to match the workspace of the task, where the other individual is interacting with the other manipulator. Thus, the motion tolerance of one individual does not affect the motion of the other. For instance, scaling down the regular workspace to match the constrained workspace can allow a helper to demonstrate a task to the individual through teleoperation. Scaling up motion from the constrained workspace to match the size of the regular workspace amplifies the individual's motion and allows him to perform the task in a workspace that he would otherwise not be able to reach.

As Fig. 3(b) suggests, the workspace mapping is not a simple linear shape scaling. Nevertheless, the goal is to map the shape of W_r into that of W_c, or vice-versa, with a non-rigid transformation that minimizes the overall distortion of the workspace to be scaled. For 2D shapes, thin plate splines interpolation has this property. It consists of an algebraic approach to the description of deformation between two surfaces specified by scattered point-preponderances (landmark points) [47].

Consider the reduced state variable $\xi = [x,y]$ defined in the Cartesian space that solely represents the 2D position of a generic point. To find the transformation $g(\xi)$ between W_r and W_c, we assume to have a set of n landmarks $\xi_r = [x_t\ y_t]^T$ in the reference shape (the coordinates of 2D points in the shape to be deformed to match a target shape), and the corresponding homologous set of n landmarks ξ_t in the target shape. This process involves deforming the reference shape such that the reference landmarks match the target landmarks, i.e., $g(\xi_r) = \xi_t$, while minimizing a bending energy function for the transformation. The function $g(x,y) \in \mathbb{R}^2 \to \mathbb{R}^2$ must be twice differentiable and minimize

$$\int\int_{\mathbb{R}^2} \left(\frac{\partial^2 g}{\partial x^2}\right)^2 + 2\left(\frac{\partial^2 g}{\partial x \partial y}\right)^2 + \left(\frac{\partial^2 g}{\partial y^2}\right)^2 dxdy. \tag{24}$$

The transformation can be written as a sum of functionals which only depend on one component of g as

$$g(x,y) = b_0 + b_1 x + b_2 y + \sum_{i=1}^{n} w_i U(\xi, \xi_{r_i}). \tag{25}$$

The first part of the above equation, $b_0 + b_1 x + b_2 y$, forms a linear flat surface corresponding to a uniform or affine

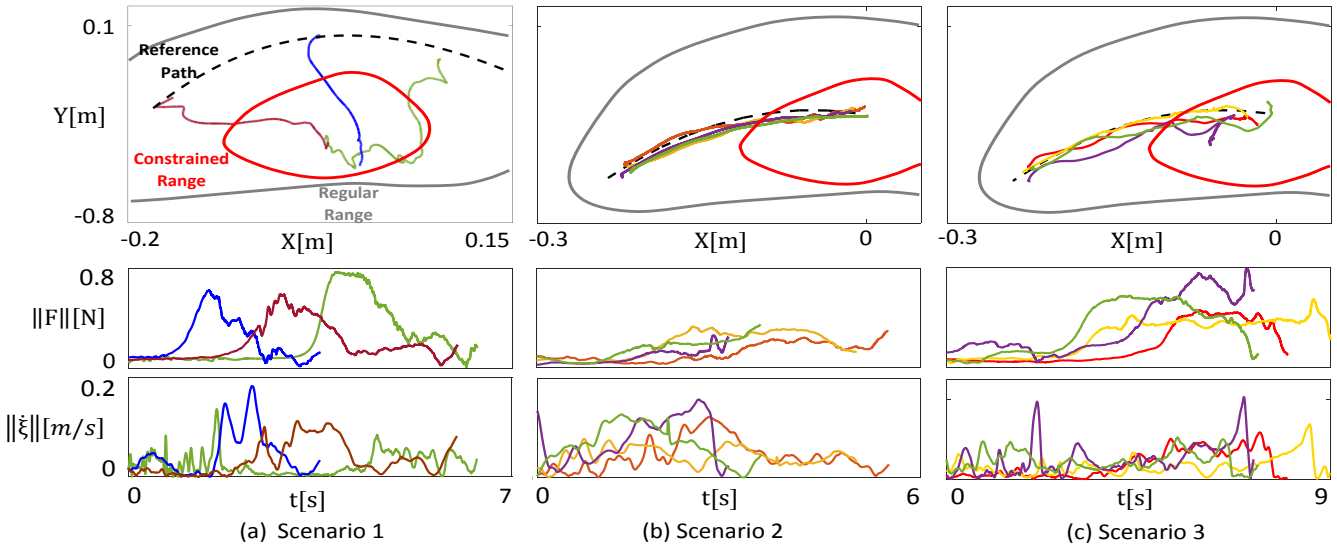

Fig. 7. First set of experimental results (Scenarios 1, 2, and 3). The first row shows the end-effector position and the task space, the second row shows the measured force and the third row shows the end-effector velocity. In (a) the results of Scenario 1 (left) and 2 (right) show how the robot stretches the individual's arm as she exits the constrained workspace. In (c), the robot opposes to the motion along the reference trajectory towards the target point.

transformation, and the second part is nonlinear (nonuniform transformation). The input to the function is the coordinate location of a generic point $\xi = [x\ y]^T$ in the reference shape and $g(x,y)$ outputs the interpolated location of ξ in the deformed shape. The coefficient vectors b_0 to $b_2 \in \mathbb{R}^{2\times 1}$ are constants to be determined later, w_i is a weighing coefficient for each of the reference landmarks, and $U(\xi, \xi_{r_i})$ is a radial basis function defined as

$$U(v_{ij}) = v_{ij}^2 \ln(v_{ij}^2), \tag{26}$$

where the value $v_{ij} = \|\xi_i - \xi_j\|$ is the Euclidean distance between points ξ_i and ξ_j, and $\ln(\cdot)$ denotes the natural logarithm function.

In order to quantify the relative amount of distortion required to match pairs of landmarks in the same shape, let $K \in \mathbb{R}^{n\times n}$ be a symmetric matrix that summarizes the distances between the n reference landmarks ξ_r, defined as

$$K = \begin{bmatrix} 0 & U(v_{12}) & \dots & U(v_{1n}) \\ U(v_{21}) & 0 & \dots & U(v_{2n}) \\ \vdots & & \ddots & \vdots \\ U(v_{n1}) & U(v_{n2}) & \dots & 0 \end{bmatrix}, \tag{27}$$

where, for example, $U(v_{12})$ is the distance between ξ_{r_1} and ξ_{r_2} given by (26). The spacing of landmarks is an important constraint because it requires more shape deformation between closely spaced landmarks than between landmarks located at a distance from one another.

Let $R \in \mathbb{R}^{n\times 3}$ be a matrix containing the n landmark points of the reference shape, i.e.,

$$R = \begin{bmatrix} 1 & 1 & \dots & 1 \\ \xi_{r_1} & \xi_{r_2} & \dots & \xi_{r_n} \end{bmatrix}^T. \tag{28}$$

To compute the weighting coefficient and the coefficient vectors b, we can now define a new matrix $L \in \mathbb{R}^{(n+3)\times(n+3)}$ as

$$L = \begin{bmatrix} K & R \\ R^T & O_1 \end{bmatrix}, \tag{29}$$

where $O_1 \in \mathbb{R}^{3\times 3}$ is a matrix of zeros. The inverse of L represents the energy required to displace the landmarks of the reference configuration in any combination and by any amount.

Now, let Q be a matrix containing the respective coordinates ξ_{t_i}, in the target configuration, of each reference landmark ξ_{r_i}, that is

$$Q = \begin{bmatrix} \xi_{t_1} & \xi_{t_2} & \dots & \xi_{t_n} & O_2 \end{bmatrix}^T,$$

where $O_2 \in \mathbb{R}^{3\times 2}$ is a matrix of zeros. The weights assigned to the uniform and nonuniform modes of shape variation (b_0 to b_2, and w_i, respectively) are determined as follows:

$$[w_1\ \dots w_n,\ b_0\ b_1\ b_2]^T = L^{-1}Q. \tag{30}$$

The corresponding location of a generic point $\xi = [x\ y]^T$ expressed in the reference shape, can now be calculated in the target shape by inputting the result of (30) in (25). Notice that if the target landmark's location is a linear scaling of the reference landmark's location, i.e., $\xi_{t_i} = c\xi_{r_i}\ \forall i$ with $c \in \mathbb{R}$, then $w_i = 0\ \forall i$ and the transformation is affine.

The next step to map the workspaces is to define landmarks in the contours or each shape. To this end, the workspaces are first centred and a set of $n_L \in \mathbb{N}$ straight lines are defined in polar coordinates. They are traced from the center of the workspaces up to point having coordinates $[\cos(\theta_L)\ \sin(\theta_L)]^T \times \rho$ where $\rho = \sqrt{2}$ is the line length and $\theta_L = 2\pi j/n_L,\ j \in \{1,2,...,n_L\}$, is the polar angle of each of the n_L lines with respect to x. The intersection of each line with the contours of the workspaces gives one pair of landmarks. An example of the transformation applied to the workspaces determined in the previous section is shown in Fig. 8.

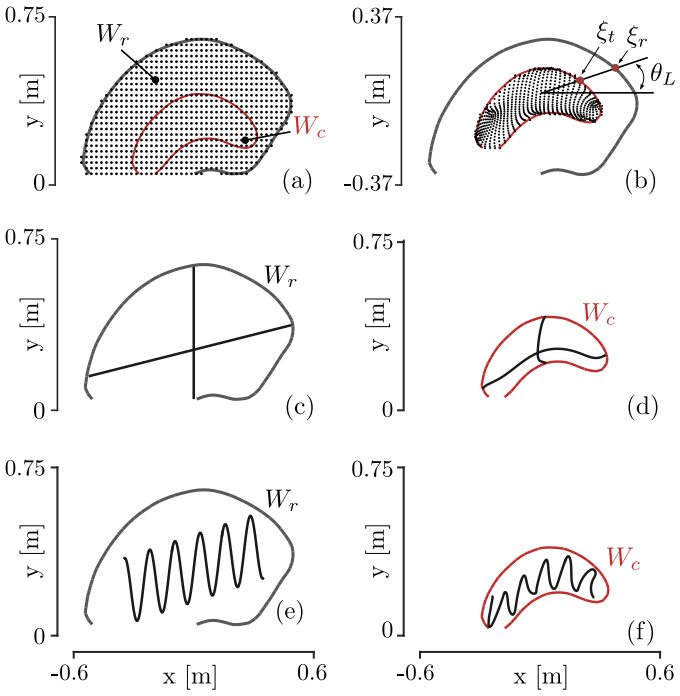

Fig. 8. Workspace mapping through thin plate spline interpolation. In (a) a random grid of points is created within the regular workspace (W_r). In (b), the center of both workspaces are aligned and pairs of landmark points are defined where the lines cross each workspace contour. 20 pairs of landmarks are used. The transformed grid defined in (a) is also shown in (b). The constrained workspace W_c is then shifted back to its origin. (d) and (f) present the result of the transformation applied to the trajectories shown in (c) and (e), respectively.

TABLE II
SUMMARY OF EXPERIMENTAL CONDITIONS FOR EACH EXPERIMENTAL SCENARIO (ES).

ES	k_1	σ
1	200	0.025
2	200	0.03
	250	0.03
3	250	0.025
4	250	0.05
	200	0.03
5	200	0.02

*Average force in [N], †Average velocity in [mm/s]

VI. Application to Assistive Robotic System

In the context of assistive robotics, motion is only performed within the constrained workspace and assistance is provided to increase accuracy in performing the task within that workspace only. A helper without movement disorders moves the robot end-effector to define a trajectory, in the helper's workspace. The temporal position of the robot's end-effector is converted to the user's workspace following the non-linear mapping. Once the converted trajectories are defined, a potential field is created to assist the individual with disabilities to be more accurate in the activity while she moves the robot end-effector. This is suitable for individuals with motion coordination impairments and movement spasms. Two new experimental

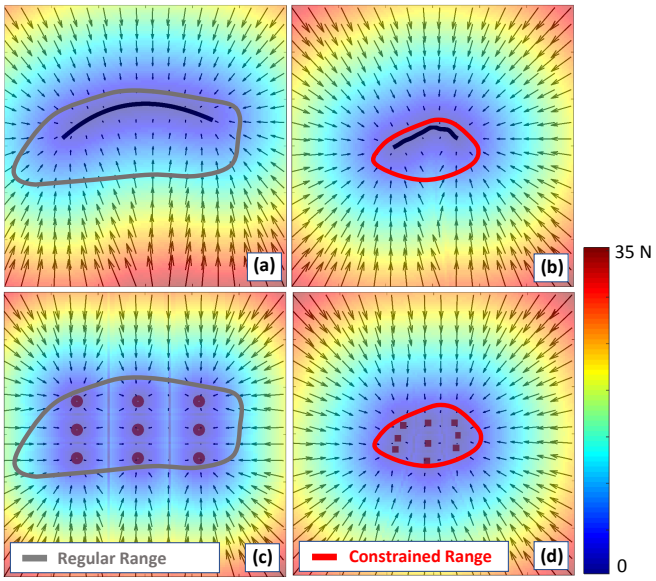

Fig. 9. Force field for Scenarios 4 (a-b) and 5 (c-d). In (a), an individual without disability defines a reference trajectory in his regular range of motion. In (b), thin plate spline interpolation scales the trajectory to the individual's range of motion and the force field is created. In (c), reference points are defined in the regular workspace and converted to the individual's workspaces in (d).

scenarios are considered:

1) **Scenario 4 - Following a trajectory**: This task consists of accurately following a desired trajectory. First, a helper without disability moves the robotic manipulator within his regular range of motion and so defines a reference trajectory (see Fig. 9(a)). Workspace mapping applied to the trajectory converts it into the one shown in Fig. 9(b), which lays within the individual with disabilities' constrained workspace. A potential field is created to help her follow the transformed trajectory. The trajectory, mapped to her constrained workspace, is displayed on the LCD monitor while she moves the robot end-effector along it.
2) **Scenario 5 - Keeping the hand still**: Inspired from a actions required during a board game, in this scenario the individual with disabilities is requested to move her hand to specific points and keep the hand still for 1 to 2 seconds before moving to the nearest next point. A grid of points initially defined in a regular workspace (Fig. 9(c)) is scaled using Thin Plate Spline (TPS) interpolation to match the individual's constrained workspace (Fig. 9(d)). A potential force field is created around the transformed grid. The grid of points, mapped to her constrained workspace, is displayed on the LCD monitor.

The following refers to the results obtained in Scenario 4. The right column of Fig. 10(a) shows the measured end-effector position (top row), the individual's applied force (middle row), and velocity (bottom row) when no assistance is provided. The individual is unable to accurately follow the trajectory for several consecutive trials. The left columns of Fig. 10(a) shows the obtained path when assistance is given by

setting $S = 3000$ and $k_1 = 0$ (as shown in Fig. 9(b)). The results of trials indicate that the individual is now able to follow the trajectory with roughly half of the deviation seen in the case without assistance. The amount of given assistance correlates to the magnitude of the robot applied force (middle row).

The experimental results from Scenario 5 are summarized in Fig. 10(b). The right column shows the measured position, the interaction force, and the velocity of the robot's end-effector when no assistance is provided ($S = 0,\ k_1 = 0$). One can observe a large deviation from each target point meaning that the individual is unable to maintain the end-effector still at the desired location in each of the six trials. In the left column of Fig. 10(b), assistance is given with $S = 3500$, $k_1 = 0$, and $\sigma = 0.04$. The robot applies force to the manipulator towards the nearest reference point. As a result, the interaction force is higher when compared to the case without assistance leading to lower deviation from the target points. This also lowers the end-effector velocity as can be seen in the third panel.

Although it is not presented in this paper, the individual's motion could be scaled back to the regular workspace using the inverse of the TPS interpolation function such that the individual and an individual without disability can collaborate during the task, each using their preferred range of motion.

VII. Discussion and Conclusion

In this study an 8-DOF model was determined and applied in rehabilitation robot and assistive robot contexts for an individual with cerebral palsy. In rehabilitation robot scenarios, the kinematic model successfully informed regions in the workspace where forces were needed for stretching, and applying assisting and resisting forces for movement therapy scenarios. In the assistive robot context, the nonlinear workspace mapping successfully tuned trajectories and force fields to the individual with cerebral palsy's range of motion based on the model; and the force fields reduced position variations, which therefore enabled the individual to be more accurate in her movements. Other rehabilitation robotics approaches have been based on generic pre-determined trajectories or motion acquired, for example, from demonstrations [13], [14], [15], [16]. The difference in our approach is that a kinematic model of the upper limb complex informs the controller about the capabilities and range of motion of the user and motion planning or assistance are then designed based on the information acquired from the model. A time-invariant potential field function was applied only outside the constrained workspace, based on the model. Likewise, the kinematic model informed the non-linear mapping, providing an extension on other approaches. For example, in [30] the non-linear mapping was performed for various predetermined shapes, whereas in this study the mapping was based on a human movement model. In [32] they mapped to the workspace of the robot rather than an individual.

In the following we discuss some limitations, features, and ways to improve upon these contributions: 1) A 8-DOF kinematic model of the upper limb, 2) a learning-from-demonstration robot-control strategy via a time-invariant potential field function, and 3) a nonlinear registration method to map different workspaces. These contributions do not depend on each other and may be used independently.

A. Kinematic model

Incorporating motor control into the kinematic model of the upper limb can open up several research avenues. When the hand moves between two points, the robotic system would be able to select one specific trajectory among a finite number of possible ones that lead to the target position. It is well known that the central nervous system selects a pathway by minimizing a given cost function [39], [48]. But what does this cost function look like? In the current form, one can clearly see that the trajectory derived from the differential inverse kinematic model is a straight path, which assumes that individuals tend to select a path that minimizes metabolic energy costs [38], [39]. Nevertheless, this is not always the case and it is possible to modify the model in order select alternative paths that minimize a combination of displacement, velocity, and/or acceleration of specific joints between those points. In the experiments reported here, for instance, it would be suitable to select a path that minimizes the total angular displacement of the elbow from its flexed position.

Optimal trajectory planning based on the kinematic model can also be used to minimize the effects of involuntary joint movements through the forward kinematic model. For instance, the robot may select a path that minimizes the manipulability of the 8-DOF model end-effector. This is equivalent to selecting a position and orientation of the arm less prone to the effects of spasms. As an insight into the structure of an unknown cost function of a specific individual, one may analyse the path followed by the hand through the inverse kinematic model, compute the joint angles, and in doing so may be able to define an approximate cost function to be implemented in robotic rehabilitation and/or assistance.

The proposed framework expects that individuals can reliably reach the same range of motion over time, which may not be the case over several trials, or on different days. Accommodating variability can be incorporated in future iterations.

B. Robot control

Manually assisted movement training and assistance lack repeatability and objective measures of individual performance and progress. In contrast, with robot-assisted therapy the duration and number of training sessions can be increased, while reducing the one-on-one therapist time required per individual. Only a short interaction of the therapist with the individual is thereby necessary since the robot is able to learn the required task-specific assistance. In the therapist's absence, the robot autonomously assists the individual when performing the same task. This, however, emphasizes a critical issue: When interacting with humans, robots must be able to deal with uncertainties and classical robot position control falls short in addressing this issue since one cannot predict the individual's behaviour.

Consider for instance variable impedance control. It is one of the most prominent control methods used to regulate the interaction between the human and the robotic manipulator. It

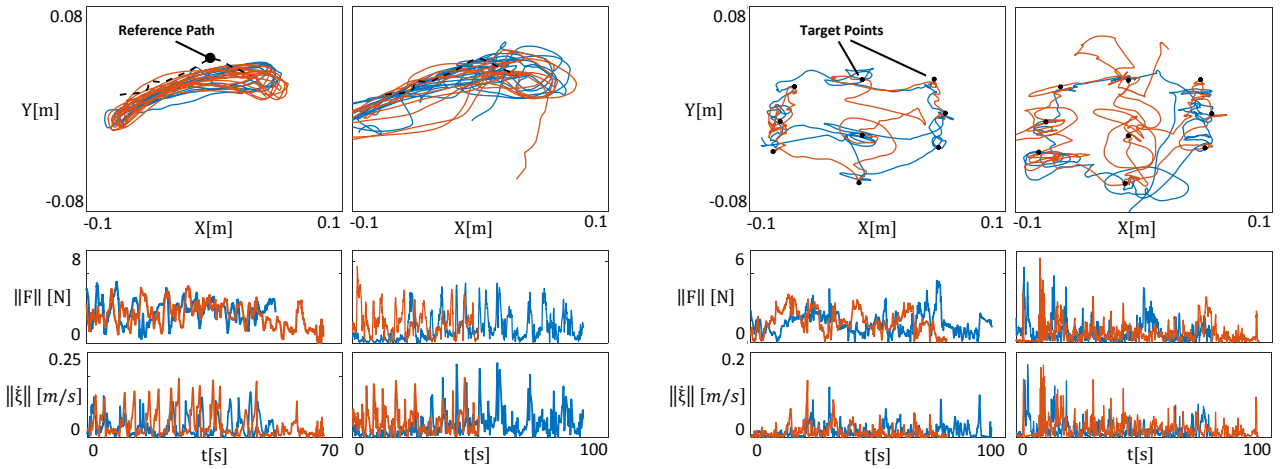

(a) Scenario 4 - Following a trajectory

(b) Scenario 5 - Keeping the end-effector still

Fig. 10. Experimental results for Scenarios 4 (a) and 5 (b). In (a), the individual tries to follow the reference trajectory with (first column) and without (second column) any assistance. In the second and third row force and velocity are shown. In (b), the objective is to keep the end-effector still for about 1-2 seconds on each of the reference points. The first and second column show the results obtained with and without assistance, respectively.

allows adapting the robot interaction properties, for instance by making it more or less compliant in uncertain regions. This class of control still relies on position control and hence, real-time motion generation that operates jointly with the controller is needed. More critical is the fact that assistance provided by these algorithms is time dependent implying that the individual is required to follow the demonstrated trajectory at a similar velocity as in the demonstration phase. Otherwise, the robot increases the applied force to drag the user's hand on the desired path. In contrast, the nonparametric potential field function used in this paper calculates the required assistive force from either therapist demonstrations or functional task and is time independent. It essentially consists of a position-to-force mapping with the force being constant at a given position. Such a time-invariant controller with bounded force ranges guarantees that the robot is stable when in contact with passive environments. Thus, if the individual deviates from the demonstrated trajectory, assistance is given to prevent further deviation from the desired trajectory, in a rate that is proportional to the observed deviation.

Combined with the kinematic model, assistance is calculated by taking into account the individual's specific motion tolerances given by joint limits. In the case of rehabilitation, one may experience sudden changes in the applied force when first exiting the constrained workspace. A low pass filter may be used in future work to present such behaviour. The proposed method is versatile and can be used in a variety of rehabilitation contexts such as resistive and assistive therapy with only minor parameter tuning.

C. Workspace mapping

The nonlinear workspace mapping between the individual's range of motion and that of an individual without disability allows both individuals to perform tasks cooperatively. Through the workspace mapping, the individual is always using her entire workspace, which is expected to promote her engagement. Individuals with more motivation in such tasks are believed to have higher motor recovery and improvement of symptoms than those described as less enthusiastic [49]. The workspace mapping and the robot controller proposed here may be combined to refine the individual's motion and reduce effects of tremor and spasms.

There are ways to improve and extend upon the presented methodology. In order to match the individual's preferred direction of motion, an additional step may be used in the scaling process to rotate the workspaces and adjust the direction of motion from one workspace to another. Tasks being performed in regions that the individual cannot reach are scaled to match her feasible range of motion, allowing both individuals to interact without posing risks or discomfort to the individual. Using the inverse of the TPS interpolation function, it is possible to scale the individual's motion back to the regular workspace such that the individual and a helper can collaborate during the task, each using his preferred range of motion. The effects of nonlinear mapping on the stability of bilateral teleoperation is an open question.

D. Final remarks

The proposed framework addresses the need to design robotic rehabilitation therapies and assistive robotics based on an individual's abilities. The kinematic model of the upper limb served as the basis to take into account an individual with cerebral palsy's abilities and provide robotic assistance within the individual's motion tolerances. Evaluation of the 8-DOF kinematic model with the individual confirms the effectiveness and benefits of the proposed framework. The kinematic model effectively informed regions in the workspace where forces were needed and applied the time-invariant potential field function in stretching, assisting and resisting rehabilitation exercises. The nonlinear workspace mapping based on the model successfully tuned trajectories and force fields to the individual with cerebral palsy's comfortable range of motion, enabling the individual to reach the desired targets and be more accurate in her movements.

ACKNOWLEDGMENTS

This research was supported by a Collaborative Health Research Project (CHRP), a joint initiative of the National Sciences and Engineering Research Council (NSERC) under grant 462227-14 and Canadian Institutes of Health Research (CIHR) under grant 134744, Canada Foundation for Innovation under grant LOF 28241, the Alberta Innovation and Advanced Education Ministry under Small Equipment Grant RCP-12-021, and by in-kind contributions from Quanser Inc. No potential conflict of interest was reported by the authors.

REFERENCES

[1] A. Rios et al., "Playfulness in children with limited motor abilities when using a robot," *Physical & Occupational Therapy in Pediatrics*, vol. 36, no. 3, pp. 232–246, 2016.

[2] N. Paneth, T. Hong, and S. Korzeniewski, "The descriptive epidemiology of cerebral palsy," *Clinics in Perinatology*, vol. 33, no. 2, pp. 251–267, 2006.

[3] H. Van der Ploeg et al., "Physical activity for people with a disability," *Sports Medicine*, vol. 34, no. 10, pp. 639–649, 2004.

[4] e. a. H. Krueger, "Prevalence of individuals experiencing the effects of stroke in canada," *Stroke*, vol. 46, no. 8, pp. 2226–2231, 2015.

[5] C. Copen, K. Daniels, and W. Mosher, "National health statistics reports," *Hyattsville, MD*, pp. 2008–2017, 2017.

[6] H. Krebs et al., "Rehabilitation robotics: pilot trial of a spatial extension for MIT-Manus," *Journal of NeuroEngineering and Rehabilitation*, vol. 1, no. 1, p. 5, 2004.

[7] E. Mohammadi, H. Zohoor, and M. Khadem, "Design and prototype of an active assistive exoskeletal robot for rehabilitation of elbow and wrist," *Scientia Iranica. Transaction B, Mechanical Engineering*, vol. 23, no. 3, p. 998, 2016.

[8] D. Centonze et al., "Repetitive transcranial magnetic stimulation of the motor cortex ameliorates spasticity in multiple sclerosis," *Neurology*, vol. 68, no. 13, pp. 1045–1050, 2007.

[9] S. E. Fasoli, H. I. Krebs, J. Stein, W. R. Frontera, and N. Hogan, "Effects of robotic therapy on motor impairment and recovery in chronic stroke," *Archives of physical medicine and rehabilitation*, vol. 84, no. 4, pp. 477–482, 2003.

[10] J. McLaughlin et al., "Selective dorsal rhizotomy: efficacy and safety in an investigator-masked randomized clinical trial," *Developmental Medicine & Child Neurology*, vol. 40, no. 4, pp. 220–232, 1998.

[11] P. Lum et al., "Robot-assisted movement training compared with conventional therapy techniques for the rehabilitation of upper-limb motor function after stroke," *Archives of physical medicine and rehabilitation*, vol. 83, no. 7, pp. 952–959, 2002.

[12] G. Prange et al., "Systematic review of the effect of robot-aided therapy on recovery of the hemiparetic arm after stroke," *Journal of rehabilitation research and development*, vol. 43, no. 2, p. 171, 2006.

[13] S. F. Atashzar, M. Shahbazi, M. Tavakoli, and R. V. Patel, "A computational-model-based study of supervised haptics-enabled therapist-in-the-loop training for upper-limb poststroke robotic rehabilitation," *IEEE/ASME Transactions on Mechatronics*, vol. 23, no. 2, pp. 563–574, 2018.

[14] L. Luo, L. Peng, C. Wang, and Z. Hou, "A greedy assist-as-needed controller for upper limb rehabilitation," *IEEE Transactions on Neural Networks and Learning Systems*, vol. 30, no. 11, pp. 3433–3443, 2019.

[15] T. Koeppel and O. Pila, "Test-retest reliability of kinematic assessments for upper limb robotic rehabilitation," *IEEE Transactions on Neural Systems and Rehabilitation Engineering*, vol. 28, no. 9, pp. 2035–2042, 2020.

[16] J. Zhang and C. C. Cheah, "Passivity and stability of human–robot interaction control for upper-limb rehabilitation robots," *IEEE Transactions on Robotics*, vol. 31, no. 2, pp. 233–245, 2015.

[17] V. Maheu et al., "Evaluation of the JACO robotic arm: Clinico-economic study for powered wheelchair users with upper-extremity disabilities," in *International Conference on Rehabilitation Robotics*, 2011, pp. 1–5.

[18] B. Graf, A. Hans, J. Kubacki, and R. Schraft, "Robotic home assistant care-o-bot ii," in *Proceedings of the Engineering in Medicine and Biology Conference*, vol. 3. IEEE, 2002, pp. 2343–2344.

[19] K. Kawamura et al., "Intelligent robotic systems in service of the disabled," *IEEE Transactions on rehabilitation engineering*, vol. 3, no. 1, pp. 14–21, 1995.

[20] M. Najafi, M. Sharifi, K. Adams, and M. Tavakoli, "Robotic assistance for children with cerebral palsy based on learning from tele-cooperative demonstration," *International Journal of Intelligent Robotics and Applications*, pp. 1–12, 2017.

[21] S. W. Brose, D. J. Weber, B. A. Salatin, G. G. Grindle, H. Wang, J. J. Vazquez, and R. A. Cooper, "The role of assistive robotics in the lives of persons with disability," *American Journal of Physical Medicine Rehabilitation*, pp. 509–521, 2010.

[22] R. J. F. van den Heuvel, M. A. S. Lexis, G. J. Gelderblom, R. M. L. Jansens, and L. P. de Witte, "Robots and ict to support play in children with severe physical disabilities: a systematic review," *Disability and Rehabilitation: Assistive Technology*, vol. 11, no. 2, pp. 103–116, 2016, pMID: 26330097. [Online]. Available: https://doi.org/10.3109/17483107.2015.1079268

[23] V. Dietz and T. Sinkjaer, "Spastic movement disorder: impaired reflex function and altered muscle mechanics," *The Lancet Neurology*, vol. 6, no. 8, pp. 725–733, 2007.

[24] F. Biering-Sørensen, J. B. Nielsen, and K. Klinge, "Spasticity-assessment: a review," *Spinal cord*, vol. 44, no. 12, pp. 708–722, 2006.

[25] J. Veneman et al., "Design and evaluation of the LOPES exoskeleton robot for interactive gait rehabilitation," *IEEE Transactions on Neural Systems and Rehabilitation Engineering*, vol. 15, no. 3, pp. 379–386, 2007.

[26] F. Vicentini et al, "Safenet: A methodology for integrating general-purpose unsafe devices in safe-robot rehabilitation systems," *Computer methods and programs in biomedicine*, vol. 116, no. 2, pp. 156–168, 2014.

[27] R. Prokopenko, A. Frolov, E. Biryukova, and A. Roby-Brami, "Assessment of the accuracy of a human arm model with seven degrees of freedom," *Journal of Biomechanics*, vol. 34, no. 2, pp. 177 – 185, 2001. [Online]. Available: http://www.sciencedirect.com/science/article/pii/S0021929000001792

[28] R. W. Bohannon and M. B. Smith, "Interrater reliability of a modified ashworth scale of muscle spasticity," *Phys ther*, vol. 67, no. 2, pp. 206–207, 1987.

[29] S. F. Atashzar, N. Jafari, M. Shahbazi, H. Janz, M. Tavakoli, R. V. Patel, and K. Adams, "Telerobotics-assisted platform for enhancing interaction with physical environments for people living with cerebral palsy," *Journal of Medical Robotics Research*, vol. 02, no. 02, p. 1740001, 2017. [Online]. Available: https://doi.org/10.1142/S2424905X17400013

[30] C. Rossa, M. Najafi, M. Tavakoli, and K. Adams, "Nonlinear workspace mapping for telerobotic assistance of upper limb in patients with severe movement disorders," in *2017 IEEE International Conference on Systems, Man, and Cybernetics (SMC)*, 2017, pp. 2255–2260.

[31] M. Sharifi, S. Behzadipour, H. Salarieh, and M. Tavakoli, "Assist-as-needed policy for movement therapy using telerobotics-mediated therapist supervision," *Control Engineering Practice*, vol. 101, p. 104481, 2020. [Online]. Available: http://www.sciencedirect.com/science/article/pii/S0967066120301106

[32] Z. Chen, S. Yan, M. Yuan, B. Yao, and J. Hu, "Modular development of master-slave asymmetric teleoperation systems with a novel workspace mapping algorithm," *IEEE Access*, vol. 6, pp. 15 356–15 364, 2018.

[33] J. Lenarcic and A. Umek, "Simple model of human arm reachable workspace," *IEEE Transactions on Systems, Man, and Cybernetics*, vol. 24, no. 8, pp. 1239–1246, Aug 1994.

[34] M. Benati et al., "Anthropomorphic robotics," *Biological Cybernetics*, vol. 38, no. 3, pp. 125–140, 1980.

[35] R. Hartenberg and J. Denavit, "A kinematic notation for lower pair mechanisms based on matrices," *Journal of applied mechanics*, vol. 77, no. 2, pp. 215–221, 1955.

[36] Y. Xia and J. Wang, "A dual neural network for kinematic control of redundant robot manipulators," *IEEE Transactions on Systems, Man, and Cybernetics, Part B (Cybernetics)*, vol. 31, no. 1, pp. 147–154, Feb 2001.

[37] L. Sciavicco and B. Siciliano, "A solution algorithm to the inverse kinematic problem for redundant manipulators," *IEEE Journal on Robotics and Automation*, vol. 4, no. 4, pp. 403–410, 1988.

[38] R. Alexander, "A minimum energy cost hypothesis for human arm trajectories," *Biological cybernetics*, vol. 76, no. 2, pp. 97–105, 1997.

[39] K. Ohta et al., "Optimal trajectory formation of constrained human arm reaching movements," *Biological cybernetics*, vol. 91, no. 1, pp. 23–36, 2004.

[40] P. Palisano, R.and Rosenbaum, D. Bartlett, and M. Livingston, "Gross motor function classification system–expanded and revised," *Can child centre for childhood disability research, Institute for Applied Health Sciences McMaster University*, 2007.

[41] A.-C. Eliasson, L. Krumlinde-Sundholm, B. Rösblad, E. Beckung, M. Arner, A.-M. Öhrvall, and P. Rosenbaum, "The manual ability classification system (macs) for children with cerebral palsy: scale development and evidence of validity and reliability," *Developmental Medicine & Child Neurology*, vol. 48, no. 7, pp. 549–554, 2006. [Online]. Available: https://onlinelibrary.wiley.com/doi/abs/10.1111/j.1469-8749.2006.tb01313.x

[42] C. Rossa, J. Lozada, and A. Micaelli, "Design and control of a dual unidirectional brake hybrid actuation system for haptic devices," *IEEE Transactions on Haptics*, vol. 7, no. 4, pp. 442–453, 2014.

[43] T. Tsuji and Y. Tanaka, "Tracking control properties of human-robotic systems based on impedance control," *IEEE Transactions on Systems, Man, and Cybernetics - Part A: Systems and Humans*, vol. 35, no. 4, pp. 523–535, July 2005.

[44] F. Ferraguti, C. Secchi, and C. Fantuzzi, "A tank-based approach to impedance control with variable stiffness," in *IEEE International Conference on Robotics and Automation*. IEEE, 2013, pp. 4948–4953.

[45] A. Blank, J. French, A. U. Pehlivan, and M. O'Malley, "Current trends in robot-assisted upper-limb stroke rehabilitation: promoting patient engagement in therapy," *Current physical medicine and rehabilitation reports*, vol. 2, no. 3, pp. 184–195, 2014.

[46] S. M. Khansari and O. Khatib, "Learning potential functions from human demonstrations with encapsulated dynamic and compliant behaviors," *Autonomous Robots*, vol. 41, no. 1, pp. 45–69, 2017.

[47] F. L. Bookstein, "Principal warps: Thin-plate splines and the decomposition of deformations," *IEEE Transactions on pattern analysis and machine intelligence*, vol. 11, no. 6, pp. 567–585, 1989.

[48] Y. Uno, M. Kawato, and R. Suzuki, "Formation and control of optimal trajectory in human multijoint arm movement," *Biological cybernetics*, vol. 61, no. 2, pp. 89–101, 1989.

[49] N. Maclean and P. Pound, "A critical review of the concept of patient motivation in the literature on physical rehabilitation," *Soc Sci Med*, vol. 50, no. 4, pp. 495–506, 2000.